Journal of
Bioengineering & Biomedical Science

Research Article Open Access

Development and Validation of Phase-Shifting Profilometry Using a Hyperspectral Spatial Frequency Domain Imaging System Integrated with a Neurosurgical Microscope

Leticia Angulo-Rodriguez[1], Youmna Badawy[1] and Frederic Leblond[1,2]*

[1]*Department of Engineering Physics, Polytechnique Montreal, CP 6079, Succursale Centre-Ville, Montreal H3C 3A7, Canada*
[2]*Centre de recherche du Centre hospitalier de l'Université de Montréal (CRCHUM), 900 rue St-Denis, Montréal, Quebec, H2X 0A9, Canada*

Abstract

Neurosurgery microscopes that detect fluorescence associated with biological tissue are used to guide tumor resection surgeries. However, they can't estimate values for tissue optical absorption and scattering needed to quantify fluorescence. An important first step to accurately assess absorption and scattering is the determination of the geometric shape of the sample. Here we present a new imaging system that performs 3D reconstructions through a neurosurgical microscope by projecting structured light. The profilometry system was evaluated using phantoms in the shape of stairs with multiple steps allowing determining 3D reconstruction accuracy and precision. The average accuracy and precision for all step heights (from 1.5 to 30 mm) was 0.3 mm and 0.6 mm, respectively. Profilometry measurements at different angles were also acquired by rotating a platform by ± 15°, 30° and 45°. The mean reconstruction error for all angles was 1.94° (STD=1.2°).

Keywords: Neurosurgery; Surgical microscope; Profilometry; Biomedical optics; Tissue optical properties; Fluorescence; Diffuse reflectance

Introduction

Surgical excision of the tumour remains the first-line therapy for most brain cancers, including gliomas [1]. For gliomas, the completeness of tumour resection is an important factor because it can have a dramatic impact on the subsequent evolution of the disease [2]. Magnetic Resonance Imaging (MRI) is used both for surgical planning and for neuro-navigation during the procedure based on either pre-operative or intra-operative imaging. However, MRI suffers from a lack of sensitivity to normal brain invaded by cancer cells, often resulting in residual cancer outside of contrast-enhancing boundaries following a surgical procedure [3]. Further, intraoperative stereovision images have shown that there is a measurement error of as much as 1 cm in target location of brain structures during surgery when compared to pre-operative MRI due in large part to brain shift [4]. These limitations are detrimental to patient safety and survival because they are responsible for a reduction in procedural accuracy and reliability.

As a result of the lack of precision and sensitivity of standard care techniques, new complementary methods were developed to assist surgeons in characterizing brain tumor margins in real time, including fluorescence-guided surgery [5] using organic fluorescence molecules like fluorescein sodium [6,7] and Indo-cyanine Green (ICG) [8]. Especially in the case of molecular tracers targeting specific cancer processes, clinical translation of these methods is enticing because they can potentially offer high contrast between healthy and cancerous tissue, as well as being safe since imaging is done using non-ionizing radiation [9]. In the past, a multicenter phase III clinical trial showed that the fluorescence from protoporphyrin IX (PpIX) resulting from the administration of exogenous 5-aminolevulinic acid (5-ALA) helped to improve the completeness of tumour resection [10]. Commercial neurosurgical microscopes were developed with an imaging mode allowing real time intraoperative PpIX fluorescence detection by using this marker as a surrogate for tumour metabolism [11]. These microscopes allow surgeons to employ a white light–for the visualization of tissue structure–from which blue light in the 400-410 nm wavelength band is filtered to excite PpIX. A filter in the detection path typically eliminates light below 620 nm for fluorescence visualization (emission at >635 nm) [12,13]. However, an important limitation of those fluorescence microscopes is that they are providing only a qualitative assessment of the fluorescence tissue levels. The intensity of the detected signal is usually proportional to the concentration of the fluorescent marker but it is non-linear in terms of the heterogeneous tissue absorption (mainly due to hemoglobin) and elastic scattering (tissue microstructure) properties. As a result, only upon correcting for the underlying absorption and scattering properties can quantified values of fluorescence be provided that are representative of the actual concentrations of fluorophores.

Several groups have developed approaches for intraoperative fluorescence quantification using hand-held reflectance/fluorescence probes [14,15] or using wide-field spectroscopic systems [15-17]. Typically the attenuation correction leading to quantified fluorescence values can be either model-based using diffuse reflectance signals to retrieve tissue optical properties [18] or based on a ratio-metric techniques using reflectance signals to normalize the fluorescence spectra [18,19]. For model-based approaches using Monte Carlo simulations or analytic solutions to the radiative transfer equation (or the diffusion equation), accurate values for the absorption coefficient must be retrieved in order to implement a correction that is precise enough not to introduce errors reducing the utility of the resulting quantified fluorescence values. Imaging techniques have

***Corresponding author:** Frederic Leblond, Department of Engineering Physics, Polytechnique Montreal, CP 6079, Succursale Centre-Ville, Montreal H3C 3A7, Canada, Tel: 514-340-4711, Ext: 4740; E-mail: frederic.leblond@polymtl.ca

Received: January 17, 2019; **Accepted:** February 01, 2019; **Published:** February 07, 2019

Citation: Angulo-Rodriguez L, Badawy Y, Leblond F (2019) Development and Validation of Phase-Shifting Profilometry Using a Hyperspectral Spatial Frequency Domain Imaging System Integrated with a Neurosurgical Microscope. J Bioengineer & Biomedical Sci 9: 257.

been developed to provide a quantitative estimate of absorption and scattering coefficients (μ_a and μ'_s) to be able to afford quantification of fluorophore concentrations during brain surgery [18]. In other work, Spatial Frequency Domain Imaging (SFDI) was used to determine μ_a and μ'_s coefficients in wide-field imaging mode [20]. SFDI works under the assumption that the optical properties set the degree of image blurring at a specific spatial frequency; Monte-Carlo simulations of image analysis and the standard diffusion theory can be then used to extract the absorption and diffusion coefficients [21]. Next, these values can be used in a wide-field quantitative fluorescence imaging model reported in [18] to quantify the intensity of fluorescence images.

However, an important ingredient missing in the neurosurgery quantified fluorescence imaging studies is the reconstruction of the 3D profile of the surgical cavity. It is essential for the quantification of μ_a and μ'_s because surface curvature is one of the factors that affect how light reflects off of biological tissue. Indeed, approaches to use the 3D surface profile to correct the fluorescence intensity map of the tissue surface have been developed elsewhere [22,14]. For instance, Gioux et al. applied a geometric correction to estimate the precise values of scattering and absorption coefficients that were used as surrogates for tissue physiological status [22]. The range of errors in depth measurements they obtained was at ~1 mm. This level of accuracy was demonstrated to be sufficient to improve computation of tissue optical properties since the geometric correction induced up to 10 fold changes in light signals. However, this work was achieved on a stand-alone imaging system and thus was not integrated with a surgical microscope.

In this work we present the development of a through-microscope wide-field hyperspectral SFDI system. Although the eventual use of the system is for PpIX or endogenous fluorescence and intrinsic absorption/scattering imaging combined with 3D brain surface profilometry, here we are presenting as proof-of-principle a validation of the optical design for computing the 3D surface profile. As explained below, the accuracy of the profilometry system was evaluated using phantoms of known heights. All the heights were reconstructed with an average relative error (the theoretical height minus the measured height, divided by the theoretical height) less than 3%. Then, the accuracy of depth measurements was determined based on an average absolute error (the difference between the theoretical and measured values) of 0.3 mm.

System Design

To ensure minimal disruption of the surgeon workflow during a procedure, the system was integrated to free optical ports of a neurosurgical microscope. As seen in Figures 1A and B, the 3D profilometer functionality was added to a commercial Zeiss NC-4 neuromicroscope (Carl Zeiss, Oberkochen, Germany) by connecting to different light channels of the same microscope eyepieces: a) A custom optical adapter allowing to project any pattern of light a few centimeters across the brain surface using a Digital Light Projector (DLP, Digital Light Innovations, TX, USA), b) An adapter (TrueTex, FL, USA) connecting (proximal end) a coherent fiber optics imaging bundle (Schott, Mainz, Germany) allowing to image over a field-of-view (FOV) consistent with that seen through the microscope. The proximal end of the bundle was connected to a liquid crystal tunable filter (LCTF, VariSpec, PerkinElmer, MA, USA) and an Electron Multiplying Charge-Coupled Device (EMCCD, Hnu model, Nuvu Cameras, Canada). The Visible wavelength (VIS) LCTF model used in this study provided continuously tunable filtering within the wavelength range from 400 to 720 nm with a bandwidth of 7 nm. The projector system was connected to a fiber-coupled single-mode laser (Oxxius, Lannion, France) with peak excitation wavelength at 638 nm. The laser was coupled to the microscope projector adaptor using a single-mode optical fiber with core diameter of 3 μm and a numerical aperture (NA) of 0.12. The illumination wavelength was chosen because light transmission of the LCTF (~ 80%) is higher at longer wavelengths (e.g. transmission is ~ 40% at 400 nm). The digital micromirror device (DMD) of the DLP was illuminated by a collimated beam to ensure uniform surface illumination and maximum light transmission across the remaining optical components in the projector and in the microscope. Moreover, before the beam illuminates the micromirrors array, it goes from the laser fiber output through optical components within the projector (mirrors, lenses) impacting differently light propagation at different wavelengths. For example, light at wavelengths lower than 638 nm diverged more within the projector due to the larger index of refraction of glass at those lower wavelengths. This directly impacted the collimation of the beam that illuminated the DMD and, in consequence, the uniformity of the image coming out of the projector which then also limited the accuracy of the profilometry system. In addition, the low numerical aperture of the microscope also constrained the passage of a more divergent beam, which could cause a major loss of optical power through the system. Finally, a single-mode laser coupled to a single mode fiber was chosen over a multimode laser because the spatial and temporal coherence of a multimode laser was creating speckles within the illumination field. These speckles led to uneven illumination while adding image noise causing inaccuracies in the 3D reconstructions.

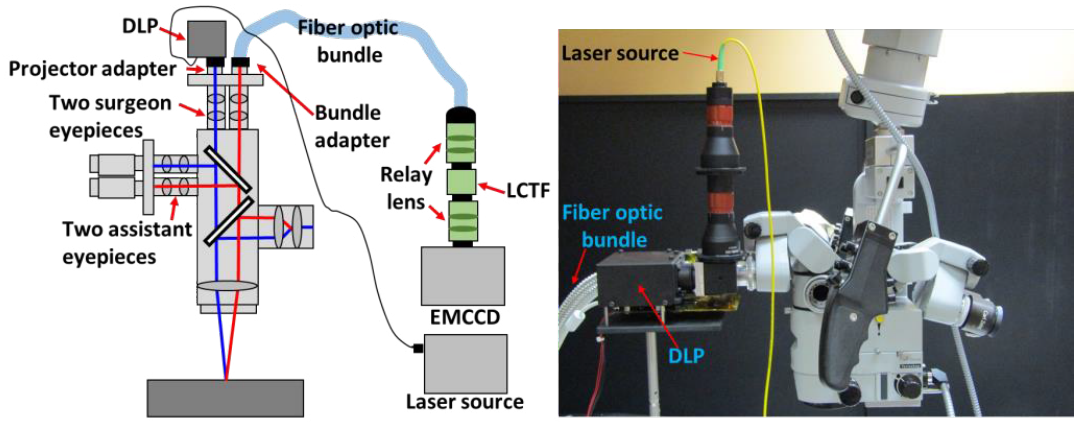

Figure 1A: Optical system to perform 3D reconstruction through a neurosurgical microscope: a DLP and a fiber optic bundle are coupled to the microscope eyepieces by means of optical adapters.

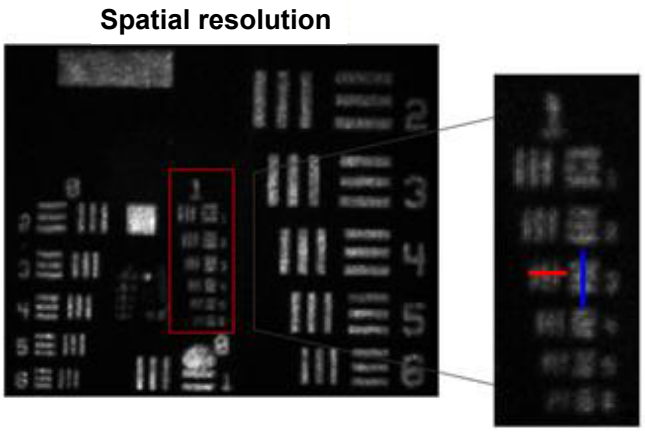

Figure 1B: Spatial Resolution.

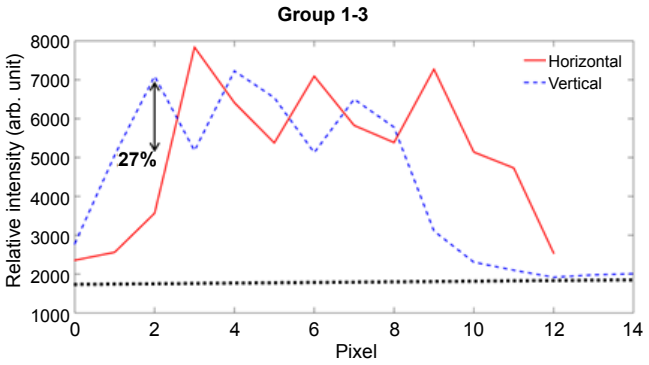

Figure 2: The finest details that the imaging system can resolve correspond to group 1-3 of an USAF 1951 resolution target.

The Zeiss NC-4 neuro-microscope used for this study had variable magnification (1-6X) and variable focal length (200-400 mm). However, here in order to test the hypothesis that 3D images of the surgical cavity can be produced through a commercial neurosurgical microscope, a focal length of 300 mm (commonly used during neurosurgery) and a magnification factor of 1X were used at a working distance of 30 cm from the microscope head lens to the image plane. A projected image then occupied an area of 4 × 3 cm in the microscope FOV. The axial resolution of the imaging system (with those imaging parameters) was evaluated based on the Rayleigh criterion using a standard 1951 USAF resolution target. That criterion was met for group 1-3 as shown in Figure 2; thus, the 2D resolution of the system is ~ 2.5 lp/mm or approximately 200 μm, which is usually considered adequate for observation of tumors at macroscopic scales [15]. The light power at 638 nm out of the fiber-coupled laser was >100 mW. However, the illumination at zero spatial frequency (uniform illumination) amounted to a fluence of 85 μW/cm^2 due to multiple sources of losses with the DMD and the microscope. Indeed, the most important limitation of the profilometry setup is that there is a 98% light loss in the system, mostly due to the very small aperture size of the microscope lenses that receive light from the DMD. This can yield images with low Signal-to-noise Ratio (SNR) which can influence significantly the performance of the phase-shifting profilometry algorithm.

The projection covers 308 by 232 pixels on the camera sensor, which corresponds to 78 pixels/cm. As explained below, although the DMD was capable of producing light patterns with a different spatial amplitude and phase modulation, the system presented here was optimized to project sine patterns at four different phase shifts: 0, π/2, π, -π/2, and spatial frequencies between 1 and 1.75 cm^{-1}.

Phase-shifting profilometry algorithm

The structured light projection setup was built ensuring it can be used in the future for intraoperative measurement of tissue optical properties corrected for the effect of surface curvature [22]. Here, to reconstruct 3D surface profiles, the four step phase-shifting profilometry algorithm [23] was implemented based on the projection of four sinusoidal-intensity fringe patterns with relative π/2 phase shifts. Depending on the profilometry method of choice, either three or four fringe patterns are projected with different phases to obtain a 3D representation of an object. However, for methods based on three phases, three reference images associated with a flat surface have to be acquired. In contrast, using a method based on four phase shifts avoids having to acquire reference images. Because of the difficulties associated with acquiring reference images during surgical procedures, this technique was adopted here. When a sine-shaped light pattern was projected, deformations ensued that can be used as a surrogate to reconstruct surface geometrical changes. Specifically, those deformations induced a change in the phase of the sine wave intensity profile (compared to a flat surface) and for any given position on the surface the resulting phase could be computed based on the intensity of the 4 deformed patterns. It is the fact that this phase value is proportional to the surface height for each individual pixel that was used to reconstruct the profile [24]. Briefly, the resulting deformed patterns were modeled with the following equations:

$$I_1(x,y) = I_a(x,y) + I_b(x,y)\cos(\phi(x,y)) \quad (1)$$

$$I_2(x,y) = I_a(x,y) - I_b(x,y)\sin(\phi(x,y)) \quad (2)$$

$$I_3(x,y) = I_a(x,y) - I_b(x,y)\cos(\phi(x,y)) \quad (3)$$

$$I_4(x,y) = I_a(x,y) + I_b(x,y)\sin(\phi(x,y)) \quad (4)$$

where I_1, I_2, I_3 and I_4 are the light intensities for pixel locations x and y associated with the four relative phase shifts: 0, π/2, π, -π/2. I_a is a constant term associated with the mean intensity for all four fringe patterns and I_b is half of the peak-to-peak amplitude of the sinusoidal component of the signals. The phase for each pixel is given by:

$$\tan(\phi(x,y)) = \frac{I_4(x,y) - I_2(x,y)}{I_1(x,y) - I_3(x,y)} \quad (5)$$

Because the phase should physically be limited to a 2π interval, a phase unwrapping algorithm was applied to ensure the range was between -π and +π [23]. For this study, the phase information was recovered after running a 2D phase unwrapping function in Matlab (The Mathworks, Inc.) [25]. Then, in order to associate a height value (in proper units of length) to each camera pixel, the size of the projected sine patterns was measured with a ruler along the x-axis to obtain an individual conversion factor (k_x). Then, knowing the total length of the illuminated region along the x-axis (L_x), it was possible to determine the length of each projected oscillation in centimeters (p):

$$p = \frac{(k_x L_X)}{\omega}[\text{cm}] \quad (6)$$

where ω is an integer representing the number of fringes. The height (h) was determined by multiplying the phase (ϕ) by the variable p and by the scaling factor (c) found with a calibration phantom of known heights (here a stair phantom was used as described below):

$$h = \phi(x,y)\, pc[\text{cm}] \quad (7)$$

In order to achieve an effective 3D reconstruction with minimized errors, the 3D profile can be created with the average of individual reconstructions. An individual reconstruction is obtained from pattern projections with a single spatial frequency; then, all the reconstructions carried out from projections with different spatial frequencies are averaged. As explained below, in this study, the average of reconstructions with spatial frequencies from 1 to 1.75 cm^{-1} proved to reconstruct effectively small and large height changes.

A C++ code was written to synchronize the projection of patterns by the DLP and the image acquisition with the LCTF/EMCCD system. An acquisition to project and acquire spatial frequency domain images in a span of frequencies of 1 to 1.75 cm^{-1} took <1 min and the processing was performed after image acquisition in <2 min.

Evaluation of depth reconstruction measurements

Experimental protocols were planned and implemented to test the ability of the instrument to create 3D surface profiles through a neurosurgical microscope as well as to evaluate the reconstruction accuracy of the method. Initially, several stair phantoms were 3D-printed with step heights varying from 1.5 mm to 30 mm (Figure 3). The height of all stair phantoms was kept to <40 mm to ensure they could all be imaged within the 40 mm depth of field of the microscope [26]. Each stair phantom was placed within the microscope FOV and structured light patterns of 4x3 cm were projected at zoom=1X and focal length=300 mm. A 3D reconstruction was obtained for each phantom after averaging reconstructions obtained for different spatial frequency projections in the 1 to 1.75 cm^{-1} range. This method was found to afford a sufficient level of sensitivity to detect all height changes associated with the phantoms. The average absolute accuracy of the profilometry system (theoretical height minus measured height) was found to be 0.3 mm. Figure 3A shows the measured heights for the different pyramid steps. The standard deviation was calculated amongst the heights estimated pixel-by-pixel across the surface of every step. The average standard deviation for all the step areas was less than 0.6 mm and this is considered to be the precision of the profilometry system. Another experiment was performed where a flat adjustable angle platform (AP180, Thorlabs) was positioned at 0° (perpendicular) with respect to the head of the surgical microscope. Then, the platform was moved at ± 15°, ± 30° and ± 45° along the x- and y-axis, creating side- and front-tilt maps, respectively, as seen in Figures 4A and 4B. The tilt accuracy is shown in Figures 4C and 4D; the mean reconstruction error for all angles was 1.9 degrees with a standard deviation of 1.2 degrees. In addition, while the 3D reconstruction accuracy and precision might stay at values close to 0.3 mm and 0.6 mm, respectively, for different microscope magnifications, changes should be expected since zoom settings in the neuromicroscope impact the size of the pattern and therefore the actual length of each projected oscillation. For that reason, in order to further validate the findings of this research, the accuracy and precision of reconstructions for other pairs of zoom and focal length should be determined by repeating the same experiments presented in this manuscript.

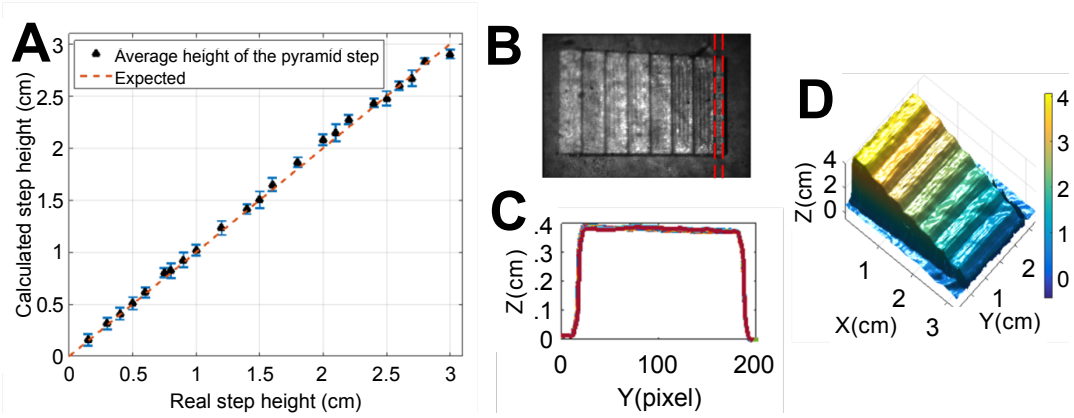

Figure 3: Height measurements made on stair phantoms: (A) Graph showing computed steps height and standard deviation (evaluated across the image for each step) as a function of expected values. (B) Reflectance image of a stair phantom with the cross-section of the first step (height: 4 mm) outlined. (C) Transverse cross-section of the step selected in (B) showing reconstructed height variability. (D) 3D surface map of the stair phantom in (B).

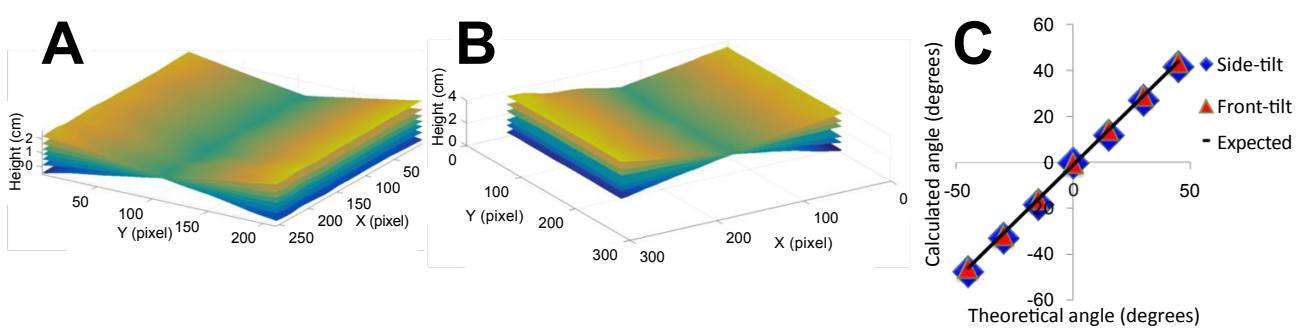

Figure 4: (A) Reconstruction of a platform rotating at different angles along the x-axis and (B) along the y-axis. (C) Measured tilt angles as a function of the expected real angles.

Finally, a brain-shaped phantom was made of intralipid, water, blue food coloring dye and agarose [27] to mimic absorption and reduced scattering coefficients of 2 mm^{-1} and 2.5 mm^{-1}, respectively, at 638 nm. The reconstructed brain profile is presented in Figure 5. However, in order to reconstruct surfaces, the sine wave patterns deformed by the shape of a sample must be perceived with enough contrast, i.e., the difference between the maximum and minimum intensities in the fringe pattern should be sufficiently high as to have easily distinguishable patterns. However, the object surface reflectance properties can vary greatly depending on geometric differences and textural features [28]. Thus, the contrast of the fringes can be low when there is irregular reflection from a non-uniform reflecting surface, hindering the 3D reconstruction of an object [29]. In consequence, despite the fact that the brain-shaped phantom was 3D reconstructed correctly, it could be the case that the patient brain surface presents large variations in reflectance, producing low contrast fringes, and making 3D reconstruction difficult. Thus, further validation of the system in a large cohort of patients shall be necessary.

Discussion

A technique was implemented to perform 3D-reconstructions without making any modification to the surgical microscope. Since each channel of the microscope oculars (eyepieces) operates as an independent optical path, the 3D profilometry functionality was developed by connecting custom optical adapters to project and detect images separately through each eyepiece.

In the presented results, spatially-modulated patterns of 4 by 3 cm were projected in the microscope FOV to carry out 3D reconstructions of calibration objects of known dimensions. Height changes were set from 1.5 to 30 mm to keep the heights within the depth of field of the neuromicroscope (40 mm) [26].

In addition, it was convenient to implement a profilometry algorithm with four phase shifts instead of three to avoid having to acquire extra sets of flat reference images during neurosurgery. The choice of spatial frequencies to perform profilometry (1 to 1.75 cm^{-1}) demonstrated enough sensitivity to detect large and small height changes. The accuracy of 3D surface reconstructions with the system was estimated to be 0.3 mm and the precision was 0.6 mm.

Finally, with the existing configuration of the through-microscope phase-shifting profilometry system presented here, sinusoidal patterns of variable spatial frequency and phase could be projected to determine μ_a and μ'_s coefficients through the SFDI technique [20]. Indeed, it has been published that the projection of structured light with a single instrument serves two purposes: 3D reconstruction of tissue structures and retrieval of its optical properties [22]. 3D profilometry information recovered with our system will be used later as prior information in a tissue light transport model for computing tissue optical properties, including scattering and absorption, during neurosurgical procedures.

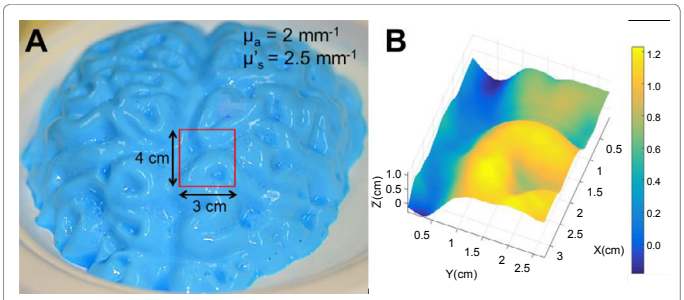

Figure 5: (A) Solid phantom with shape of brain tissue. (B) 3D reconstruction of the region-of-interest in (A).

Conclusion

A proof-of-concept study was presented suggesting that a hyperspectral imaging system that is integrated to a commercial surgical microscope can do 3D reconstructions of the brain cavity. The same setup has the potential to extract and geometrically correct the brain optical properties to quantitatively estimate fluorophore concentrations in the future which could improve cancer detection during brain surgeries.

Funding

This work was supported by the Canadian Foundation for Innovation (CFI) and the Discovery Grant program from the Natural Sciences and Engineering Research Council of Canada (NSERC).

References

1. Poulon F, Mehidine H, Juchaux M, Varlet P, Devaux B, et al. (2017) Optical properties, spectral, and lifetime measurements of central nervous system tumors in humans. Sci Rep 7:13995.
2. Stummer W, Reulen HJ, Meinel T, Pichlmeier U, Schumacher W, et al. (2008) Extent of resection and survival in glioblastoma multiforme: identification of and adjustment for bias. Neurosurgery 62:564-576.
3. LeRoux PD, Winter TC, Berger MS, Mack LA, Wang K, et al. (1994) A comparison between preoperative magnetic resonance and intraoperative ultrasound tumor volumes and margins. J Clin Ultrasound 22:29-36.
4. Fan X, Ji S, Hartov A, Roberts DW, Paulsen KD (2014) Stereovision to MR image registration for cortical surface displacement mapping to enhance image-guided neurosurgery. Med Phys 41:102302.
5. Nagaya T, Nakamura YA, Choyke PL, Kobayashi H (2017) Fluorescence-Guided Surgery. Front Oncol 7:314.
6. Okuda T, Kataoka K, Taneda M (2007) Metastatic brain tumor surgery using fluorescein sodium: technical note. Minim Invasive Neurosurg 50:382-384.
7. Uzuka T, Takahashi H, Fuji Y (2007) [Surgical strategy for malignant glioma resection with intraoperative use of fluorescein Na]. No Shinkei Geka 35:557-562.
8. Haglund MM, Berger MS, Hochman DW (1996) Enhanced Optical Imaging of Human Gliomas and Tumor Margins. Neurosurgery 38:308-317.
9. Xi L, Jiang H (2016) Image-guided surgery using multimodality strategy and molecular probes. Wiley Interdiscip. Rev Nanomed Nanobiotechnol 8:46-60.
10. Stummer W, Pichlmeier U, Meinel T, Wiestler OD, Zanella F, et al. (2006) Fluorescence-guided surgery with 5-aminolevulinic acid for resection of malignant glioma: a randomised controlled multicentre phase III trial. Lancet Oncol 7: 392-401.
11. Pogue BW,Gibbs-Strauss S, Valdes PA, Samkoe K, Roberts DW, et al. (2010) Review of Neurosurgical Fluorescence Imaging Methodologies. IEEE J Sel Top Quantum Electron 16: 493-505.
12. Bravo JJ, Olson JD, Davis SC, Roberts DW, Paulsen KD, et al. (2017) Hyperspectral data processing improves PpIX contrast during fluorescence guided surgery of human brain tumors. Sci Rep 7:9455.
13. Kim A, Khurana M, Moriyama Y, Wilson BC (2010) Quantification of in vivo fluorescence decoupled from the effects of tissue optical properties using fiber-optic spectroscopy measurements. J Biomed Opt 15:067006.
14. Haj-Hosseini N, Richter J, Andersson-Engels S, Wårdell K (2009) Optical touch pointer for fluorescence guided glioblastoma resection using 5-aminolevulinic acid. Lasers Surg Med 42: 9-14.
15. Gebhart SC, Thompson RC, Mahadevan-Jansen A (2007) Liquid-crystal tunable filter spectral imaging for brain tumor demarcation. Appl Opt 46:1896-1910.
16. Valdes PA, Jacobs VL, Wilson BC, Leblond F, Roberts DW, et al. (2013) System and methods for wide-field quantitative fluorescence imaging during neurosurgery. Opt Lett 38: 2786-2788.

17. Jermyn M, Gosselin Y, Valdes PA, Sibai M, Kolste K, et al. (2015) Improved sensitivity to fluorescence for cancer detection in wide-field image-guided neurosurgery. Biomed Opt Express 6: 5063-5074.

18. Sibai M, Veilleux I, Elliott JT, Leblond F, Wilson BC (2015) Quantitative spatial frequency fluorescence imaging in the sub-diffusive domain for image-guided glioma resection. Biomed Opt Express 6:4923.

19. Valdés PA, Leblond F, Jacobs VL, Wilson BC, Paulsen KD, et al. (2012) Quantitative, spectrally-resolved intraoperative fluorescence imaging. Sci Rep 2:798.

20. Cuccia DJ, Bevilacqua F, Durkin AJ, Ayers FR, Tromberg BJ (2009) Quantitation and mapping of tissue optical properties using modulated imaging. J Biomed Opt 14:24012-24013.

21. Cuccia DJ, Bevilacqua F, Durkin AJ, Tromberg BJ (2005) Modulated imaging: quantitative analysis and tomography of turbid media in the spatial-frequency domain. Opt Lett 30:1354-1356.

22. Gioux S, Mazhar A, Cuccia DJ, Durkin AJ, Tromberg BJ (2009) Three-dimensional surface profile intensity correction for spatially modulated imaging. J Biomed Opt 14: 034045.

23. Malacara D (2007) Optical Shop Testing. Hoboken, John Wiley & Sons, Incorporated, USA.

24. Rastogi PK, Erwin H (2012) Optical methods for solid mechanics: a full-field approach. Weinheim: Wiley.

25. Gdeisat M, Lilley F (2011) Two-Dimensional Phase Unwrapping Problem.

26. Elliott JT, Dsouza AV, Marra K, Pogue BW, Roberts DW, et al. (2016) Microdose fluorescence imaging of ABY-029 on an operating microscope adapted by custom illumination and imaging modules. Biomed Opt Express 7:3280-3288.

27. Haj-Hosseini N, Kistler B, Wårdell K (2014) Development and characterization of a brain tumor mimicking fluorescence phantom. Proc. SPIE 8945: 894505–894507.

28. Chen LC, Tsai LH (2011) Dual Phase-shifting Moiré Projection with Tunable High Contrast Fringes for Three-Dimensional Microscopic Surface Profilometry. Phys Procedia 19:67-75.

29. Chen LC, Duong DH, Chen CS (2015) 3-D Surface Profilometry for Objects Having Extremely Different Reflectivity Regions. The 14th IFToMM World Congress.